Letters

A Noninvasive Grid Impedance Estimation Method With Phase-Lock Loops

Haoxin Yang, *Member, IEEE*, and Yi Tang, *Senior Member, IEEE*

***Abstract*—For grid-following inverters, an accurate grid impedance estimation (GIE) enables many beneficial applications. Conventional active GIE methods, such as the PQ variation method, intentionally introduce power disturbances around the system's steady-state operating point. However, it might bring undesired reactive power into the grid and its accuracy can be influenced by phase-lock loop (PLL) phase angle variations. To address these challenges, this letter proposes a noninvasive GIE method, which utilizes PLL's inherent operating characteristics. It only requires a single steady-state operating point transition that naturally occurs during the system's normal operation, eliminating the need to inject deliberate PQ disturbances. In addition, by considering PLL phase angle variations, this method also ensures accurate estimation results across diverse conditions. Experimental verifications are provided, which demonstrate the effectiveness and accuracy of the proposed method.**

***Index Terms*—Grid-following inverter (GFI), grid impedance, noninvasive estimation, phase-lock loop (PLL), PQ variations.**

I. Introduction

With the ongoing emphasis on reducing carbon footprints, renewable energy generation systems and energy storage systems are receiving heightened attention and are being more widely integrated into power systems [1]. These power-electronics-based systems commonly connect to the grid via grid-following inverters (GFIs) at the point of common coupling (PCC), and their performance is inevitably influenced by grid impedance, affecting power transfer, passive component resonance, and synchronization stability [2], [3], [4]. Consequently, an accurate grid impedance estimation (GIE) has garnered extensive attention and finds applications in areas such as islanding detection, adaptive control implementations, and real-time impedance-based stability assessment [4], [5], [6].

GIE methods can be generally categorized into two groups: passive and active approaches [7]. Passive approaches enable impedance estimation by exploring existing information in the system. For example, grid inductance can be measured using current switching ripples or current distortions caused by dead-time effects [8], [9]. Alternatively, Duan et al. [10] proposed a method for identifying grid inductance by calculating the oscillation frequencies of grid currents in the transient state. However, these methods typically depend on high-bandwidth sampling and noise filtering techniques. In addition, they often overlook the grid resistance.

Active methods intentionally induce a disturbance in the grid after which grid impedance can be estimated by analyzing the consequent current responses. For example, a pulsed signal injection approach and a recursive least square algorithm were used to measure the grid impedance [11]. Alternatively, a pseudorandom binary sequence signal injection scheme was proposed to improve GIE accuracies in nonideal grid conditions [12]. Recently, a zero-sequence voltage injection GIE method was adopted in a three-phase four-wire GFI [13]. While these active methods may offer higher estimation accuracy than their passive counterparts, they undeniably pose potential power quality concerns.

For GFIs, the PQ variation method offers another active approach for GIE that brings fewer power quality concerns. This technique estimates grid impedance by intentionally changing the system's active and reactive power, thereby avoiding the need for harmonic injections [14], [15], [16], [17], [18]. To facilitate calculations, a frame transformation is typically employed to convert measured ac signals into dc signals within the *dq*-frame [7]. Building on this, a decoupled power injection strategy was proposed in [15], where only active power is adjusted when estimating the grid resistance, and only reactive power is varied for estimating the grid inductance. Moreover, an online, event-based PQ variation GIE method was proposed in [16], which involves the continuous monitoring of the positive-sequence amplitude of PCC voltages. Recently, this method was adopted in a multi-inverter system to save real-time communications [17]. However, despite their simplicity, most PQ variation techniques still require at least two PQ perturbation injections and may introduce undesired reactive power to the grid.

Moreover, it is crucial to note that the phase angle variations of phase-lock loops (PLLs) will influence the accuracy of the PQ variation estimation method. Specifically, for GFIs, the measured voltages and currents align with the PCC-voltage *dq*-frame. This frame is typically provided by a PLL, which regulates the *q*-axis PCC-voltage to zero, giving a reference synchronous phase for signal measurements and

Manuscript received 8 February 2024; revised 8 March 2024; accepted 25 March 2024. Date of publication 8 April 2024; date of current version 20 June 2024. *(Corresponding author: Yi Tang.)*

Haoxin Yang is with the Energy Research Institute, Nanyang Technological University, Singapore 639798 (e-mail: haoxin.yang@ntu.edu.sg).

Yi Tang is with the School of Electrical and Electronic Engineering, Nanyang Technological University, Singapore 639798 (e-mail: yitang@ntu.edu.sg).

Color versions of one or more figures in this article are available at https://doi.org/10.1109/TPEL.2024.3385434.

Digital Object Identifier 10.1109/TPEL.2024.3385434

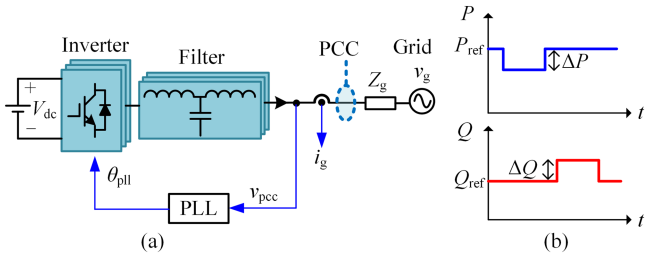

Fig. 1. Diagrams of (a) a GFI that connects to the grid at PCC with a PLL and (b) a typical PQ variation scheme for GIE.

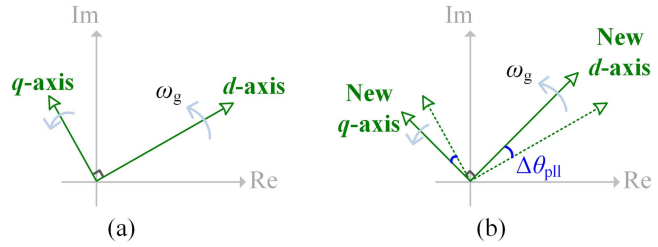

Fig. 2. Phasor diagrams of the PLL dq-frame established by PCC-voltages (a) before PQ variation and (b) after PQ variation, where the $\Delta\theta_{\rm pll}$ is the PLL phase angle variation.

injections. However, in the presence of grid impedance, the PQ variations inevitably cause steady-state changes to the PCC voltages, leading to a PLL frequency drift during the transient state. Consequently, after the PQ variations, the measured signals align with a different dq-frame. It can compromise the estimation accuracy if this effect is overlooked. Meng-Chun et al. [18] proposed a PQ variation method based on a virtual reference axis, which intentionally sets the PLL angular frequency as a constant, ensuring all measured signals align the same dq-frame during estimation. While this improves accuracy, it changes PLL's internal configurations and disables its closed-loop regulation.

To overcome the limitations of conventional methods, this letter proposes a noninvasive GIE method for GFIs based on PLL's inherent characteristics. Its major benefits are as follows.

1) The proposed method utilizes the system's natural steady-state transitions to identify both grid resistance and inductance, without injecting deliberate PQ disturbances.
2) The proposed method utilizes PLL's inherent operating characteristics, eliminating the need to change existing hardware or software configurations. Furthermore, it takes into account PLL phase angle variations, guaranteeing precise estimation results across diverse conditions.

The rest of the letter is organized as follows. Section II briefly reviews PQ variation-based GIE methods, highlighting how PLL phase angle variations influence the accuracy of the estimations. Section III introduces the proposed noninvasive GIE method, along with a practical implementation guideline. The experimental results are presented in Section IV. Finally, Section V concludes this letter.

II. PQ Variation-Based GIE Methods and PLL Phase Angle Variations

This section briefly reviews the principles of PQ variation-based GIE methods, highlighting how PLL phase angle variations impact the accuracy of the estimations. The system structure diagram is shown in Fig. 1(a), illustrating a GFI that is connected to the grid at PCC. Within this structure, $V_{\rm dc}$ is the dc-link voltage; $i_{\rm g}$ represents the grid currents; $v_{\rm pcc}$ and $v_{\rm g}$ denote the PCC voltages and grid voltages, respectively. The grid impedance, represented by $Z_{\rm g}$, comprises the grid equivalent resistance $R_{\rm g}$ and equivalent inductance $L_{\rm g}$, i.e.,

$$Z_{\rm g} = R_{\rm g} + j\omega_{\rm g} L_{\rm g} \tag{1}$$

where $\omega_{\rm g}$ represents the grid angular frequency. Fig. 1(b) shows a typical PQ variation scheme for GIE, which intentionally disturbs the system output power (specifically, the grid currents) around the system's steady-state operating points. By employing Kirchhoff's voltage law, the pre-disturbance $v_{\rm pcc}$ can be expressed as

$$v_{\rm pcc} = v_{\rm g} + i_{\rm g} Z_{\rm g}. \tag{2}$$

When $i_{\rm g}$ changes to $i_{\rm g} + \Delta i_{\rm g}$, (2) is rewritten as

$$v_{\rm pcc} + \Delta v_{\rm pcc} = v_{\rm g} + (i_{\rm g} + \Delta i_{\rm g}) Z_{\rm g} \tag{3}$$

where $\Delta v_{\rm pcc}$ denotes the PCC voltage change. Based on (2) and (3), $Z_{\rm g}$ can be determined as

$$Z_{\rm g} = \Delta v_{\rm pcc} / \Delta i_{\rm g}. \tag{4}$$

Transformation techniques are commonly employed to convert time-varying ac signals in the abc-frame into time-invariant dc signals in the dq-frame to facilitate calculations [7]. By doing so, the estimation of $Z_{\rm g}$ changes to

$$Z_{\rm g} = \Delta v_{\rm pcc\_dq} / \Delta i_{\rm g\_dq} \tag{5}$$

where $\Delta v_{{\rm pcc}\_dq}$ and $\Delta i_{{\rm g}\_dq}$ represent the PCC voltage and current changes in dq-frame, respectively. However, this result overlooks the impacts of PLL phase angle variations, which can affect the estimation accuracy. Specifically, the measured signals align with the PCC-voltage dq-frame. As shown in Fig. 1, this frame is provided by a PLL, which naturally regulates $v_{{\rm pcc}\_q} = 0$ in the steady state, thereby establishing a reference phase $\theta_{\rm pll}$ for frame transformations, signal measurements and disturbance injections. However, as indicated in (2) and (3), the PQ variations inevitably cause steady-state changes to $v_{\rm pcc}$, bringing a PLL frequency drift during the transient state. As a result, after the PQ variations, the measured signals align with a different dq-frame, exhibiting a phase angle difference (represented as $\Delta\theta_{\rm pll}$ hereinafter) compared to the original dq-frame.

The effect of this PLL phase angle variation is shown in Fig. 2, indicating that the relationship among the variables, pre- and post-PQ variations, is geometric rather than simply algebraic. Therefore, estimation results derived from a direct subtraction of the variables before and after the disturbance, as outlined in (5), are prone to inaccuracies.

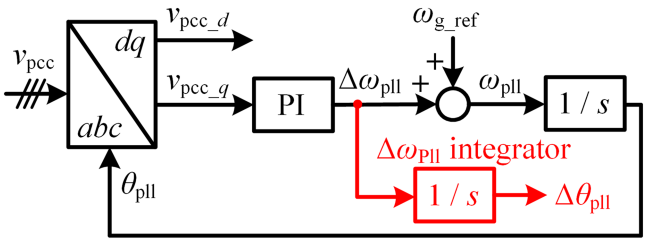

Fig. 3. Block diagram of an SRF-PLL with the $\Delta\theta_{\rm pll}$ measurement by the $\Delta\omega_{\rm pll}$ integrator.

III. Proposed Noninvasive GIE Method

A. $\Delta\theta_{pll}$ Measurement Scheme by PLLs

The $\Delta\theta_{\rm pll}$ caused by PQ variations and PLL regulations leads to estimation inaccuracies. Thus, having prior information of $\Delta\theta_{\rm pll}$ is important for an accurate GIE.

First of all, the structure of a synchronous reference frame PLL (SRF-PLL) is shown in Fig. 3, where the PLL loop filter, i.e., the PI controller, and a voltage-controlled oscillator, viz., the integrator, collectively adjust $\theta_{\rm pll}$ to attenuate $v_{\rm pcc\_q}$. Note that in the steady state, $\omega_{\rm pll}=\omega_{\rm g}$, $v_{\rm pcc\_q}=0$, and $v_{\rm pcc\_d}=V_{\rm pcc}$ are satisfied, where $V_{\rm pcc}$ denotes the magnitude of $v_{\rm pcc}$. Based on Fig. 3, $\theta_{\rm pll}$ can be determined in the s-domain as

$$\theta_{\rm pll}(s)=\omega_{\rm g\_ref}/s+\Delta\omega_{\rm pll}(s)/s. \tag{6}$$

As seen, $\theta_{\rm pll}$ comprises two components. The first component is the integration of $\omega_{\rm g\_ref}$, which provides a constant angular frequency to the reference dq-frame. As $\omega_{\rm g\_ref}$ is unchanged, this component remains unaffected by PQ variations and, consequently, does not contribute to $\Delta\theta_{\rm pll}$. The second component is the integration of $\Delta\omega_{\rm pll}$, which determines $\Delta\theta_{\rm pll}$. Specifically, when PQ variations cause changes to $v_{\rm pcc}$, $v_{\rm pcc\_q}$ will deviate from zero in the transient period. In response to this deviation, the PI controller's output, i.e., $\Delta\omega_{\rm pll}$, causes a small angular frequency drift to adjust $\theta_{\rm pll}$, aiming to reduce $v_{\rm pcc\_q}$. Consequently, in the system's subsequent steady state with $v_{\rm pcc\_q}=0$, the phase shift accumulated by $\Delta\omega_{\rm pll}$ establishes $\Delta\theta_{\rm pll}$, that is

$$\Delta\theta_{\rm pll}(s)=\Delta\omega_{\rm pll}(s)/s. \tag{7}$$

Based on (7), in order to solely obtain $\Delta\theta_{\rm pll}$, an external integrator, hereafter referred to as the $\Delta\omega_{\rm pll}$ integrator, is added to $\Delta\omega_{\rm pll}$. As depicted in the red block in Fig. 3, this addition does not alter the existing operations of the PLL. By doing so, one can easily obtain $\Delta\theta_{\rm pll}$ from this integrator's output after the PQ variations.

B. Working Principles of the Proposed GIE Method

In this section, the working principles of the proposed GIE method are presented. For clarity, $v_{\rm g}$ is chosen as a reference of zero degree, denoted as

$$v_{\rm g}=V_{\rm g}\angle 0 \tag{8}$$

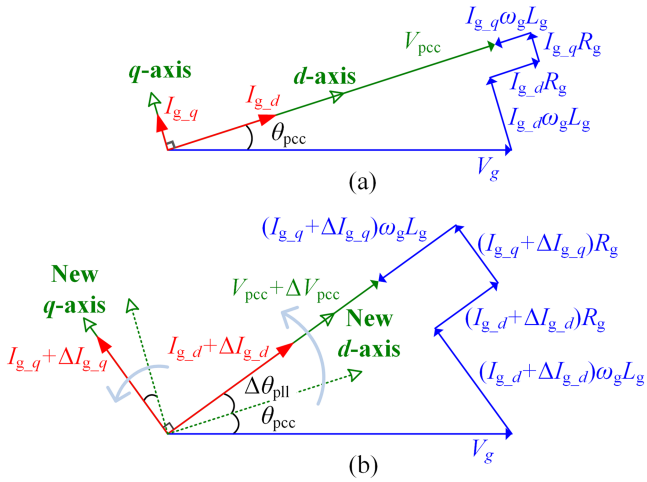

Fig. 4. Phasor diagrams of PCC voltages, grid currents, and grid voltages (a) before variation and (b) after variation.

where $V_{\rm g}$ represents the magnitude of the grid voltage. Using this reference, $v_{\rm pcc}$ can be represented as

$$v_{\rm pcc}=V_{\rm pcc}\angle\theta_{\rm pcc} \tag{9}$$

where $\theta_{\rm pcc}$ is the initial phase angle of $v_{\rm pcc}$. It is important to highlight that $\theta_{\rm pcc}$ determines the steady-state phase angle of the reference dq-frame. Based on that, $i_{\rm g}$ can be expressed as

$$i_g=I_{\rm g\_d}\angle\theta_{\rm pcc}+I_{\rm g\_q}\angle(\theta_{\rm pcc}+\pi/2) \tag{10}$$

where $I_{\rm g\_d}$ and $I_{\rm g\_q}$ are the magnitudes of currents in the d- and q-axes, respectively. Based on (1) and (2), the interrelationships among the above variables are illustrated in a phasor diagram, as shown in Fig. 4(a), where the magnitude of each phasor is labeled adjacent to its representation. Based on Fig. 4(a), one can obtain that

$$V_{\rm g}\cos(\theta_{\rm pcc})+I_{\rm g\_d}R_{\rm g}-I_{\rm g\_q}\omega_{\rm g}L_{\rm g}=V_{\rm pcc} \tag{11}$$

$$V_{\rm g}\sin(\theta_{\rm pcc})=I_{\rm g\_d}\omega_{\rm g}L_{\rm g}+I_{\rm g\_q}R_{\rm g}. \tag{12}$$

When there is a change in the steady-state working point, characterized by $\Delta I_{\rm g\_d}$ and $\Delta I_{\rm g\_q}$ that represent the changes in the d- and q-axes current magnitudes, respectively, the PCC voltage shifts to

$$v'_{\rm pcc}=(V_{\rm pcc}+\Delta V_{\rm pcc})\angle(\theta_{\rm pcc}+\Delta\theta_{\rm pll}) \tag{13}$$

where $\Delta V_{\rm pcc}$ is the PCC voltage magnitude change, and $\Delta\theta_{\rm pll}$ is the PLL phase angle variation. Aligning with a new dq-frame established by $v'_{\rm pcc}$, thus, the steady-state grid current changes to

$$\begin{aligned} i'_{\rm g}=&(I_{\rm g\_d}+\Delta I_{\rm g\_d})\angle(\theta_{\rm pcc}+\Delta\theta_{\rm pll})\\ &+(I_{\rm g\_q}+\Delta I_{\rm g\_q})\angle(\theta_{\rm pcc}+\Delta\theta_{\rm pll}+\pi/2). \end{aligned} \tag{14}$$

Subsequently, this results in modifications to the phasor diagram in the steady state, as depicted in Fig. 4(b), from which one can obtain that

$$V_g\cos(\theta_{\rm pcc}+\Delta\theta_{\rm pll})+(I_{\rm g\_d}+\Delta I_{\rm g\_d})R_{\rm g}-(I_{\rm g\_q}+\Delta I_{\rm g\_q})\omega_{\rm g}L_{\rm g}$$

$$= V_{\text{pcc}} + \Delta V_{\text{pcc}} \tag{15}$$

$$V_g \sin(\theta_{\text{pcc}} + \Delta\theta_{\text{pll}}) = (I_{\text{g\_d}} + \Delta I_{\text{g\_d}})\omega_{\text{g}} L_{\text{g}} + (I_{\text{g\_q}} + \Delta I_{\text{g\_q}}) R_{\text{g}} \tag{16}$$

Note that both V_{pcc} and $V_{\text{pcc}}+\Delta V_{\text{pcc}}$ can be obtained from $\text{v}_{\text{pcc\_}d}$ before and after the variation. Furthermore, $\Delta\theta_{\text{pll}}$ can be obtained using the $\Delta\omega_{\text{pll}}$ integrator, as shown in Fig. 3. Therefore, based on the four sets of equations, denoted as (11), (12), (15), and (16), and the four corresponding unknowns, namely, R_{g}, L_{g}, V_{g}, and θ_{pcc}, it is feasible to derive exact analytical solutions for the grid impedance, written as (17) and (18) at the bottom of this page. Particularly, for the GFIs working with a unity power factor, one can insert $I_{\text{g\_}q} = \Delta I_{\text{g\_}q} = 0$ into (17) and (18), then we obtain the following:

$$R_{\text{g},|\text{PF}|=1} = \frac{(\Delta V_{\text{pcc}} I_{\text{g\_}d} + V_{\text{pcc}} \Delta I_{\text{g\_}d} + 2V_{\text{pcc}} I_{\text{g\_}d})[1-\cos(\Delta\theta_{\text{pll}})] + \Delta V_{\text{pcc}} \Delta I_{\text{g\_}d}}{2\left(I_{\text{g\_}d}^2 + I_{\text{g\_}d}\Delta I_{\text{g\_}d}\right)[1-\cos(\Delta\theta_{\text{pll}})] + \Delta I_{\text{g\_}d}^2} \tag{19}$$

$$\omega_{\text{g}} L_{\text{g},|\text{PF}|=1} = -\frac{\Delta V_{\text{pcc}} I_{\text{g\_}d} - V_{\text{pcc}} \Delta I_{\text{g\_}d}}{2\left(I_{\text{g\_}d}^2 + I_{\text{g\_}d}\Delta I_{\text{g\_}d}\right)[1-\cos(\Delta\theta_{\text{pll}})] + \Delta I_{\text{g\_}d}^2} \sin(\Delta\theta_{\text{pll}}). \tag{20}$$

C. Practical Implementation Guideline

This section gives a practical implementation guideline for the proposed method.

Note that (17) and (18) offer a generalized estimation result that incorporates PLL phase angle variations. This enables the system to accurately identify both R_{g} and L_{g} with only one transition between any two steady states, specifically from ($I_{\text{g\_}d}$, $I_{\text{g\_}q}$) to ($I_{\text{g\_}d}+\Delta I_{\text{g\_}d}$, $I_{\text{g\_}q}+\Delta I_{\text{g\_}q}$). Such a transition commonly occurs in practical applications, such as when distributed generation systems adjust current references based on higher level

controllers, or when energy storage systems change their steady states in response to commands from energy management systems. Therefore, the proposed method can leverage these existing and natural steady-state transitions to estimate grid impedance, without causing any perturbations to the system's normal operation. From this perspective, the proposed method is noninvasive.

For conventional methods, utilizing these natural steady-state transitions is restricted, primarily because they overlook $\Delta\theta_{\text{pll}}$. Specifically, without the knowledge of $\Delta\theta_{\text{pll}}$, a single transition is not sufficient to obtain both R_{g} and L_{g}, necessitating additional information. Moreover, as $\Delta\theta_{\text{pll}}$ is not considered, their accuracy is limited to scenarios with minor steady-state transitions, where $\Delta\theta_{\text{pll}}$ is negligible. Typically, conventional methods inject two PQ distributions around the steady-state working point intentionally [14], [15], [16], [17], which is done in an invasive manner.

TABLE I
KEY SYSTEM PARAMETERS

Symbol	Value	Symbol	Value
V_{g}	110 V (rms)	ω_{g}	314 rad/s
V_{dc}	400 V	f_{sw}	20 kHz
R_{g}	1 Ω	L_{g}	4.4 mH
$V_{\text{th\_}q}$	0.5 V	$T_{\text{th\_}q}$	200 ms

A step-by-step implementation guideline for the proposed GIE method is given as follows, where the compensation for the grid frequency variation is included.

Step I: Check whether $\omega_{\text{g\_ref}} = \omega_{\text{g}}$. If yes, then proceed to Step III. If not, proceed to Step II.

Step II: When $\omega_{\text{g\_ref}} \neq \omega_{\text{g}}$, there is a dc-bias in $\Delta\omega_{\text{pll}}$. In this case, one can manually set a new $\omega_{\text{g\_ref}}$ that equals to ω_{g}. When the dc-bias of $\Delta\omega_{\text{pll}}$ reduces to zero, then proceed to Step III.

Step III: Record $I_{\text{g\_}d}$, $I_{\text{g\_}q}$, and V_{pcc} from $\text{v}_{\text{pcc\_}d}$. Then, set the initial value of the $\Delta\omega_{\text{pll}}$ integrator to zero. After that, proceed to Step IV.

Step IV: Based on the commands issued by higher level controllers, the current references in d- and q-axes change to $I_{\text{g\_}d}$ + $\Delta I_{\text{g\_}d}$ and $I_{\text{g\_}q}$ + $\Delta I_{\text{g\_}q}$, respectively. When the system reaches a new steady state and $|\text{v}_{\text{pcc\_}q}|$ is smaller than a given threshold voltage $\text{V}_{\text{th\_}q}$ for a period $T_{\text{th\_}q}$, then proceed to Step V.

Step V: Record $V_{\text{pcc}}+\Delta V_{\text{pcc}}$ from $\text{v}_{\text{pcc\_}d}$, and $\Delta\theta_{\text{pll}}$ from the $\Delta\omega_{\text{pll}}$ integrator. Then, calculate R_{g} and L_{g} based on (17) and (18), or (19) and (20). It is worth noting that one can adopt the first-order Taylor approximation into (17)–(20) for small $\Delta\theta_{\text{pll}}$ values, i.e., $\sin(\Delta\theta_{\text{pll}}) \approx \Delta\theta_{\text{pll}}$ and $\cos(\Delta\theta_{\text{pll}}) \approx 1$, to simplify the calculations [19].

IV. EXPERIMENTAL RESULTS

The effectiveness and accuracy of the proposed GIE method were tested and evaluated in this section. In the performed experiments, the grid voltage is provided by a Chroma grid emulator 61830. The three-phase GFI is fed by a bidirectional dc power supply ITECH IT600B, and the digital controller is implemented with TI TMS320F28377. The key system parameters are listed in Table I, where the total grid equivalent resistance and inductance are 1 Ω and 4.4 mH, respectively.

$$R_{\text{g}} = \frac{(\Delta V_{\text{pcc}} I_{\text{g\_}d} + V_{\text{pcc}} \Delta I_{\text{g\_}d} + 2V_{\text{pcc}} I_{\text{g\_}d})[1-\cos(\Delta\theta_{\text{pll}})] + (V_{\text{pcc}} \Delta I_{\text{g\_}q} - \Delta V_{\text{pcc}} I_{\text{g\_}q}) \sin(\Delta\theta_{\text{pll}}) + \Delta V_{\text{pcc}} \Delta I_{\text{g\_}d}}{2(I_{\text{g\_}d}^2 + I_{\text{g\_}q}^2 + I_{\text{g\_}d}\Delta I_{\text{g\_}d} + I_{\text{g\_}q}\Delta I_{\text{g\_}q})[1-\cos(\Delta\theta_{\text{pll}})] + 2\,(I_{\text{g\_}d}\Delta I_{\text{g\_}q} - \Delta I_{\text{g\_}d} I_{\text{g\_}q}) \sin(\Delta\theta_{\text{pll}}) + \Delta I_{\text{g\_}d}^2 + \Delta I_{\text{g\_}q}^2} \tag{17}$$

$$\omega_g L_{\text{g}} = -\frac{(\Delta V_{\text{pcc}} I_{\text{g\_}q} + V_{\text{pcc}} \Delta I_{\text{g\_}q} + 2V_{\text{pcc}} I_{\text{g\_}q})[1-\cos(\Delta\theta_{\text{pll}})] + (\Delta V_{\text{pcc}} I_{\text{g\_}d} - V_{\text{pcc}} \Delta I_{\text{g\_}d}) \sin(\Delta\theta_{\text{pll}}) + \Delta V_{\text{pcc}} \Delta I_{\text{g\_}q}}{2(I_{\text{g\_}d}^2 + I_{\text{g\_}q}^2 + I_{\text{g\_}d}\Delta I_{\text{g\_}d} + I_{\text{g\_}q}\Delta I_{\text{g\_}q})[1-\cos(\Delta\theta_{\text{pll}})] + 2\,(I_{\text{g\_}d}\Delta I_{\text{g\_}q} - \Delta I_{\text{g\_}d} I_{\text{g\_}q}) \sin(\Delta\theta_{\text{pll}}) + \Delta I_{\text{g\_}d}^2 + \Delta I_{\text{g\_}q}^2} \tag{18}$$

TABLE II
THREE CASES OF SYSTEM OUTPUT CURRENT VARIATIONS

	I_{g_d}	I_{g_q}	ΔI_{g_d}	ΔI_{g_q}
Case I	-5 A	-5 A	15 A	20 A
Case II	20 A	10 A	0 A	-20 A
Case III	2 A	0 A	8 A	0 A

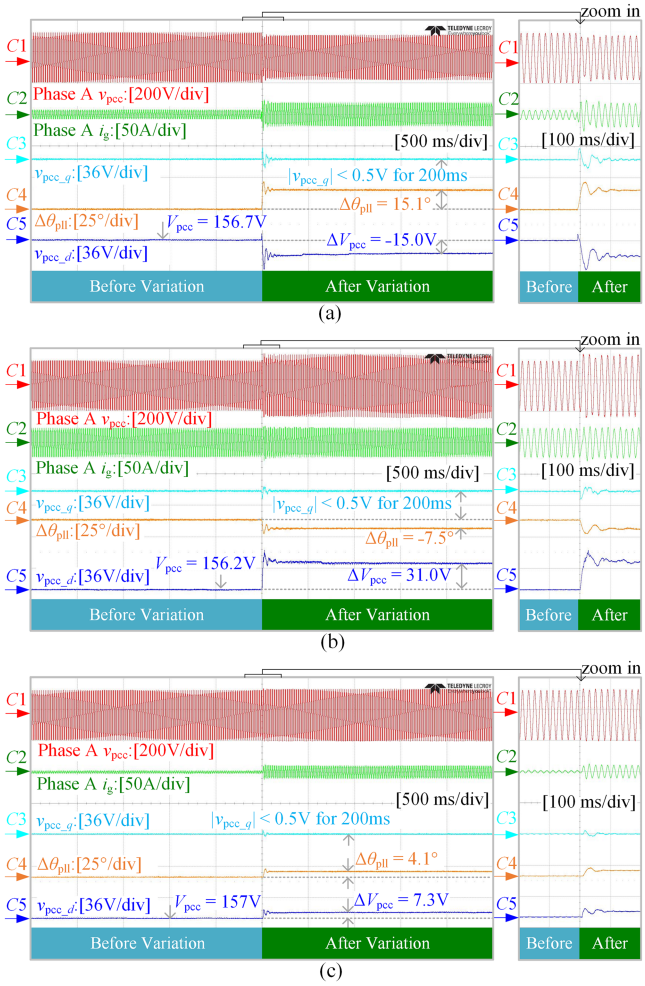

Fig. 5. Experimental waveforms of v_{pcc}, i_g, v_{pcc_q}, v_{pcc_d}, and $\Delta\theta_{pll}$ in (a) Case I, (b) Case II, and (c) Case III.

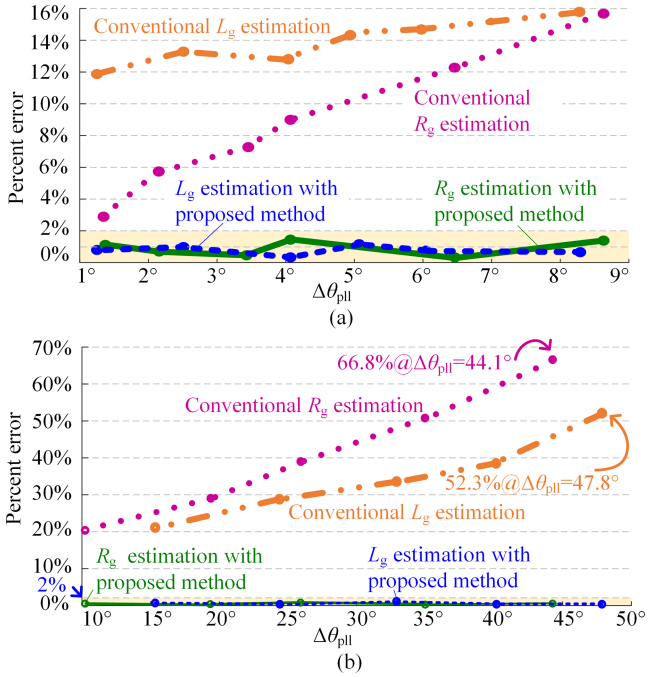

Fig. 6. Percent error of L_g and R_g estimations across various $\Delta\theta_{pll}$ with and without the proposed method (the $\Delta\theta_{pll}$ is introduced by various ΔI_{g_q} and ΔI_{g_d} in Case II and Case III, respectively), when (a) $V_g = 110$ V rms and (b) $V_g = 40$ V rms.

In Table II, three cases of the system's output states and their respective variations are given. These variations aim to emulate different natural steady-state transitions that occur during the system's normal operation.

Fig. 5(a) shows the experimental waveforms of v_{pcc}, i_g, v_{pcc_q}, v_{pcc_d}, and $\Delta\theta_{pll}$ in Case I, where v_{pcc_q}, v_{pcc_d}, and $\Delta\theta_{pll}$ are measured at the outputs of digital-to-analog chips at the controller board. As can be seen, v_{pcc} varies with i_g in the presence of R_g and L_g, bringing transient in v_{pcc_q}. After PLL's regulation, the system will achieve a new steady state when v_{pcc_q} returns to zero. Based on (17) and (18), R_g and L_g are estimated as 0.997 Ω and 4.411 mH in this case, with percent error only being 0.3% and 0.25%, respectively. It should be highlighted that conventional PQ variation-based GIE methods cannot be applied in this case, as they require separate perturbations in ΔI_{g_d} and ΔI_{g_q}. In this case, the percent error of R_g and L_g estimation using the first-order Taylor approximation, i.e., $\sin(\Delta\theta_{pll}) \approx \Delta\theta_{pll}$ and $\cos(\Delta\theta_{pll}) \approx 1$, amounts to 5.0% and 6.3%, respectively. Furthermore, the total calculation time for deriving (17) and (18) is approximately 412 ns, while for the approximation results, it is significantly reduced to about 78 ns. It should be noted that the decision to utilize the approximations also depends on the specific requirements for estimation accuracies.

Fig. 5(b) shows the experimental waveforms in Case II, where only reactive power is varied. Based on (17) and (18), R_g and L_g are estimated as 0.995 Ω and 4.362 mH, with percent error only being 0.5% and 0.86%, respectively. In contrast, the conventional PQ variation-based GIE methods can only estimate L_g in this case. Moreover, their accuracies are limited as $\Delta\theta_{pll}$ is not considered. Fig. 6(a) illustrates the comparative percent error of L_g estimation between the proposed and conventional GIE methods in this case. As seen, the proposed method exhibits a consistently low percent error, lower than 2%, under all testing conditions. In contrast, the traditional method demonstrates a significantly higher percent error, varying from 11.9% to 15.8%.

Fig. 5(c) shows the experimental waveforms in Case III, where only active power is generated and varied. Based on (19) and (20), R_g and L_g are estimated as 0.987 Ω and 4.407 mH in this case, with percent error only being 1.3% and 0.2%, respectively. This result verifies that the proposed method can accurately identify both R_g and L_g solely through a single transition in active power, without requiring any injections of reactive power. This characteristic significantly enhances the practicability of the

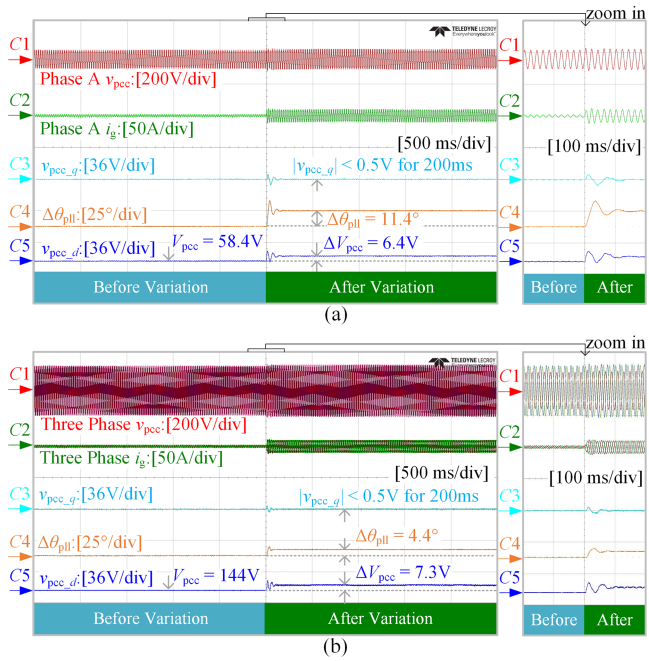

Fig. 7. Experimental waveforms of v_{pcc}, i_{g}, $v_{\mathrm{pcc\_}q}$, $v_{\mathrm{pcc\_}d}$, and $\Delta\theta_{\mathrm{pll}}$ in Cased III when the grid is under (a) a low-voltage fault ($V_{\mathrm{g}} = 40$V rms) and (b) an unbalanced voltage fault (110 V rms for phase B and C, 80 V rms for phase A).

proposed method in distributed generation systems and energy storage systems. In contrast, the conventional methods can only estimate R_{g} in this case. Fig. 6(a) also illustrates the comparative percent error of R_{g} estimation, where the proposed method still exhibits low percent errors under all testing conditions. However, the conventional method's percent error climbs significantly, even reaching as high as 15.7% at $\Delta\theta_{\mathrm{pll}} = 8.6°$.

When grid frequency changes to 50.5 Hz, R_{g} is also accurately estimated as 1.005, 0.998, and 1.011 Ω in Cases I–III with percent errors of only 0.5%, 0.2%, and 1.1%, respectively; L_{g} is estimated as 4.387, 4.422, and 4.342 mH in Cases I–III, with percent errors of only 0.3%, 0.5%, and 1.3%, respectively. These results verify the proposed method's effectiveness under grid frequency variations by following the step-by-step implementation guideline given in Section III.

Fig. 7(a) shows the experimental waveforms in Case III under a low grid voltage fault ($V_{\mathrm{g}} = 40$ V rms). In this scenario, R_{g} and L_{g} are estimated to be 1.007 Ω and 4.413 mH, with percent errors of only 0.7% and 0.3%, respectively. Under this grid condition, an enlarged $\Delta\theta_{\mathrm{pll}}$ can be more easily obtained. Therefore, Fig. 6(b) presents a more distinct percent error comparison across a wider $\Delta\theta_{\mathrm{pll}}$ range. As shown, the proposed method still consistently maintains all percent errors below 2%, in stark contrast to the conventional methods, which results in R_{g} estimation errors as high as 66.8% when $\Delta\theta_{\mathrm{pll}} = 44.1°$, and L_{g} estimation errors reaching up to 52.3% when $\Delta\theta_{\mathrm{pll}} = 47.8°$.

Fig. 7(b) shows the experimental waveforms in Case III under an unbalanced grid voltage fault (110 V rms for phases B and C, and 80 V rms for phase A), where the proposed method still works effectively by using positive sequence component extraction techniques in the PLL [20]. In this case, R_{g} and L_{g} are estimated to be 0.995 Ω and 4.430 mH, with percent errors of only 0.5% and 0.7%, respectively. These results validate the proposed method's effectiveness under grid voltage variations.

V. Conclusion

A noninvasive GIE method for GFIs is proposed in this letter. This method utilizes a natural steady-state transition to estimate both grid resistance and inductance, without causing any intentional perturbations to the grid. Note that such a transition commonly occurs in practical applications, such as when distributed generation systems adjust current references based on higher level controllers, or when energy storage systems change their steady states in response to commands from energy management systems.

Furthermore, the proposed method only uses PLL's inherent operating characteristics, eliminating the need to change PLL's existing configurations. In addition, PLL phase angle variations are considered, guaranteeing precise estimation results across diverse conditions.

The experimental results verify the proposed method's effectiveness. Specifically, it consistently maintains a percent error below 2% when $\Delta\theta_{\mathrm{pll}}$ varies from 1.2° to 47.8°. In contrast, traditional methods exhibit significantly higher estimation errors. R_{g} estimation errors can be as high as 66.8% when $\Delta\theta_{\mathrm{pll}}$ is 44.1°. Similarly, L_{g} estimation errors can reach up to 52.3% when $\Delta\theta_{\mathrm{pll}}$ is 47.8°. In addition, following the proposed step-by-step implementation guideline, our method also shows a percent error below 2% under grid frequency or voltage variations.

The first-order Taylor approximation can be applied to simplify calculations of (17)–(20), where the total computation time can be reduced by around 80% in our experimental setup. However, it is important to note that when higher estimation precision is needed, or $\Delta\theta_{\mathrm{pll}}$ is not minimal, this approximation may not be suitable. In such cases, the computational load becomes a critical factor to consider for real-time applications.

References

[1] Y. Gu and T. C. Green, "Power system stability with a high penetration of inverter-based resources," in *Proc. IEEE*, vol. 111, no. 7, pp. 832–853, Jul. 2023.

[2] X. F. Wang, L. Harnefors, and F. Blaabjerg, "Unified impedance model of grid-connected voltage-source converters," *IEEE Trans. Power Electron.*, vol. 33, no. 2, pp. 1775–1787, Feb. 2018.

[3] M. Liserre, R. Teodorescu, and F. Blaabjerg, "Stability of photovoltaic and wind turbine grid-connected inverters for a large set of grid impedance values," *IEEE Trans. Power Electron.*, vol. 21, no. 1, pp. 263–272, Jan. 2006.

[4] R. Teodorescu, M. Liserre, and P. Rodriguez, *Grid Converters for Photovoltaic and Wind Power Systems*. Hoboken, NJ, USA: Wiley, 2011.

[5] M. Cespedes and J. Sun, "Adaptive control of grid-connected inverters based on online grid impedance measurements," *IEEE Trans. Sustain. Energy.*, vol. 5, no. 2, pp. 516–523, Apr. 2014.

[6] R. Luhtala, T. Roinila, and T. Messo, "Implementation of real-time impedance-based stability assessment of grid-connected systems using MIMO-identification techniques," *IEEE Trans. Ind. Appl.*, vol. 54, no. 5, pp. 5054–5063, Sep./Oct. 2018.

[7] M. K. D. Meerendre, E. Prieto-Araujo, K. H. Ahmed, O. Gomis- Bellmunt, L. Xu, and A. Egea, "Review of local network impedance estimation techniques," *IEEE Access*, vol. 8, pp. 213647–213661, 2020.

[8] B. Arif, L. Tarisciotti, P. Zanchetta, J. C. Clare, and M. Degano, "Grid parameter estimation using model predictive direct power control," *IEEE Trans. Ind. Appl.*, vol. 51, no. 6, pp. 4614–4622, Nov./Dec. 2015.

[9] D. D. Reigosa, F. Briz, C. B. Charro, and J. M. Guerrero, "Passive islanding detection using inverter nonlinear effects," *IEEE Trans. Power Electron.*, vol. 32, no. 11, pp. 8434–8445, Nov. 2017.

[10] S. Duan, B. Xia, G. Yan, N. Li, G. Li, and Y. Ding, "A grid inductance detection method based on the oscillation characteristic of inverter terminal voltage," *IEEE Trans. Power Electron.*, vol. 37, no. 6, pp. 7209–7217, Jun. 2022.

[11] A. Suárez, C. Blanco, P. García, Á. Navarro-Rodríguez, and J. M. C. Rodríguez, "Grid impedance estimator for active multisource AC grids," *IEEE Trans. Smart Grid*, vol. 14, no. 3, pp. 2023–2033, May 2023.

[12] P. Zhong, J. Sun, L. Qu, P. Yu, and X. Zha, "An improved PRBS-injection based grid impedance measurement method considering nonideal grid conditions," *IEEE Trans. Ind. Electron.*, vol. 70, no. 6, pp. 6452–6456, Jun. 2023.

[13] Y. Cheng et al., "Zero-sequence voltage injection-based grid impedance estimation method for three-phase four-wire dc/ac grid-connected inverter," *IEEE Trans. Ind. Electron.*, early access, Aug. 23, 2023, doi: 10.1109/TIE.2023.3306395.

[14] M. Ciobotaru, R. Teodorescu, P. Rodriguez, A. Timbus, and F. Blaabjerg, "Online grid impedance estimation for single-phase grid-connected systems using PQ variations," in *Proc. IEEE 38th Power Electron. Specialists Conf.*, 2007, pp. 2306–2312.

[15] J. H. Cho, K. Y. Choi, Y. W. Kim, and R. Y. Kim, "A novel P-Q variations method using a decoupled injection of reference currents for a precise estimation of grid impedance," in *Proc. IEEE Energy Convers. Congr. Expo.*, 2014, pp. 5059–5064.

[16] N. Mohammed, T. Kerekes, and M. Ciobotaru, "An online event-based grid impedance estimation technique using grid-connected inverters," *IEEE Trans. Power Electron.*, vol. 36, no. 5, pp. 6106–6117, May 2021.

[17] N. Mohammed, T. Kerekes, and M. Ciobotaru, "Communication-free equivalent grid impedance estimation technique for multi-inverter systems," *IEEE Trans. Ind. Electron.*, vol. 70, no. 2, pp. 1542–1552, Feb. 2023.

[18] Y. Meng-Chun, C. Zhe-Yan, C. Yaow-Ming, and H. Chih-Chao, "Online grid impedance measurement based on virtual reference axis," in *Proc. Int. Power Electron. Conf.*, 2022, pp. 1504–1510.

[19] D. G. Zill, *Advanced Engineering Mathematics*. Burlington, MA, USA: Jones & Bartlett Publishers, 2020.

[20] S. Golestan, J. M. Guerrero, and J. C. Vasquez, "Three-phase PLLs: A review of recent advances," *IEEE Trans. Power Electron.*, vol. 32, no. 3, pp. 1894–1907, Mar. 2017.